JOURNAL OF CATALYSIS **176,** 14–24 (1998)
ARTICLE NO. CA982000

Protonated Sites on Sulfate-Promoted Zirconium Oxide Catalysts: A Fourier Transform-IR, Thermal Analysis, and Solid State ^{1}H NMR Study

Donald F. Stec,[1] Robert S. Maxwell,[2] and Herman Cho

Environmental Molecular Sciences Laboratory MS K8-98, Pacific Northwest National Laboratory, P.O. Box 999, Richland, Washington 99352
E-mail: hm.cho@pnl.gov

Received February 7, 1997; revised December 15, 1997; accepted January 12, 1998

A series of sulfate-promoted ZrO_2 solid acid catalysts samples were prepared, each sample differing only in the pH of the sulfuric acid soaking step of the synthesis procedure. Fourier-transform infrared (FTIR) spectra and thermal weight-loss measurements (as measured by thermal gravimetric analysis (TGA)) indicate that the pH of the sulfuric acid soaking solution influences the number of surface proton sites. The activity of sulfate-promoted ZrO_2 in catalyzing the isomerization of n-butane to iso-butane at 220°C and the surface area of the calcined catalyst are also found to depend on the soaking solution pH, with maximum surface areas and activities observed between pH 6 and pH 9. Proton nuclear magnetic resonance (NMR) chemical shifts measured using combined rotation and multiple pulse spectroscopy indicate that the sulfating step produces proton species that are more acidic than proton sites on the nonsulfated support. The proton NMR spectra of these samples consist of at least two overlapped, but distinct, resonances that can be separated on the basis of a large disparity in spin-lattice (T_1) relaxation times. By comparing the experimental spectra with a series of simulated spectra, the long T_1 component has been assigned to a discrete three- or four-proton site that includes one water molecule, and the short T_1 component to an ill-defined cluster of protons. Variable-temperature NMR lineshape data also suggest that the protons are in rapid motion on the sulfate-promoted zirconium oxide surface.

INTRODUCTION

According to some workers, sulfate-promoted zirconium oxides are effective catalysts for isomerization reactions (1–3) because they are superacidic (4–8). A recent report (9), however, contends that the high catalytic activity arises not from superacidity, but from the ability of sulfate-promoted zirconia to stabilize transition state complexes at the surface. Some authors claim that the catalytic activity can be attributed to Brønsted acid sites (10–12), while others propose that the catalyzed reaction takes place at strong Lewis acid sites (13, 14).

These catalysts have been studied by a variety of techniques (15–25) with much of the current knowledge about the structure of acid sites inferred from infrared (IR) spectroscopic studies (16, 21–25). Through the use of probe molecules, such as CO and pyridine, multiple Lewis acid sites have been distinguished and assigned to either coordinatively unsaturated zirconium (Zr^{3+}, Zr^{4+}), support sites (21–24), or to surface sulfate species (25). The Brønsted acid sites have been found to consist of both terminal and bridging hydroxyl groups (21–25). Proton nuclear magnetic resonance (NMR) (26, 27), temperature programmed desorption (28, 29), and theoretical (30) studies of unpromoted ZrO_2 powders and surfaces have shown that undissociated molecular water and assorted hydoxyl species are also present on the ZrO_2 surface. A series of studies by Dumesic and coworkers has established that the catalytic activity of sulfated zirconia catalysts is correlated with the concentration of both hydroxyl acid sites and molecular water (31–33).

The evidence that multiple, closely spaced hydrogen atoms are associated with catalytically active acid sites, of both the Brønsted type and Lewis type, suggests that proton NMR spectra can play a valuable role in determining the identity and structure of these sites, unperturbed by the introduction of foreign probe molecules. Multinuclear magic angle spinning (MAS) NMR (20, 34, 35) has been used to determine the presence of multiple Lewis acid sites with varying acidities in sulfate-promoted zirconium oxide and has shown that the Lewis sites on sulfate-promoted zirconium oxide are more acidic than those on unpromoted zirconium oxide catalysts (18). Brønsted acid sites have also been detected previously using ^{1}H MAS NMR (6, 9, 35–38). A single broad resonance centered at 6 ppm has been assigned to the acidic

[1] Present address: Department of Chemical Engineering, Stanford University, Stanford, CA 94305-5025.

[2] Present address: Analytical Sciences Division, Lawrence Livermore National Laboratory, P.O. Box 808/L-226, Livermore, CA 94551.

0021-9517/98 $25.00

protons on sulfate-promoted zirconium oxide, and, in addition, Mastikhin *et al.* (35) have observed peaks at 1.3 and 6.3 ppm that they have assigned to surface water and acidic protons, respectively.

Despite their value in making the proton chemical shifts of solid samples more easily resolved, MAS and more sophisticated combined rotation and multiple-pulse spectroscopy (CRAMPS (39)) experiments suppress spectral features, such as dipolar splittings and anistropic chemical shift lineshapes, that also contain useful data about the environment and dynamics of the observed nuclei. Past proton NMR work has made little use of the information contained in the homonuclear dipolar features of the proton NMR lineshape to deduce the structure of hydrogenated acid sites on the surface of sulfated zirconia. In this paper, the measurement and interpretation of these other parameters, in combination with FT-IR, thermal analyses, and activity studies, are used to elucidate the identity and arrangement of protons in hydrogenated sites associated with the catalytic activity of sulfate-promoted zirconia. This approach can be used to extract parameters, such as interproton distances, on the unperturbed structure of protonated sites that are unavailable from other types of measurements. Such data provide an experimental reference for direct comparison with hypothetical models of hydrogenated active sites. In one such model, proposed by Clearfield *et al.* (40), the uncalcined catalyst contains multiple proton sites in the form of hydroxyl groups located on both the bisulfate group and on the zirconium support. Calcining results in the removal of water and the formation of both Brønsted and Lewis acid sites. Some Lewis acid centers are formed with bisulfate groups left intact with an adjacent S−O−H group. We present evidence demonstrating that this model, unlike other plausible models, is consistent with the dipolar lineshapes in the proton NMR spectra.

We have prepared a series of samples for these studies, each sample differing in the pH of the soaking solution that was used in the sulfation step. In addition to the NMR experiments, these samples were probed by a number of techniques to determine if the pH of the soaking solution affects properties such as surface area, surface density of acid sites, or other parameters that could in turn be manipulated to optimize catalyst performance. According to these results, the soaking solution pH that seems to optimize the properties of the catalyst lies in the range pH 6 to pH 9.

METHODS

Catalyst Synthesis

The zirconium hydroxide support was prepared following a method (22) consisting of the dropwise addition of 1 *M* NH_4OH to 4 *M* zirconyl chloride hydrate ($ZrOCl_2 \cdot 8H_2O$). The slurry was then filtered, washed with hot distilled water to complete removal of chloride anion in the filtrate, and dried for 12 h at 120°C. The amorphous product was then dried at a pressure of 10^{-3} torr and a temperature of 120°C for 8 h. Sulfate-promoted samples were prepared by mixing 1 g of support with 30 ml of 1 *M* H_2SO_4 while stirring for 2 h. The slurry was filtered and dried for 12 h at 120°C. The powder catalyst was then dried at 120°C under vacuum for 8 h.

Two additional sets of samples were prepared by a similar procedure, but with the 1 *M* H_2SO_4 soaking solution adjusted to higher pH values by addition of either 1 *M* NH_4OH or 1 *M* NaOH. Because of the addition of base, the concentration of the counterion, SO_4^{2-}, varied according to soaking solution pH, with solutions at higher pH values containing lower SO_4^{2-} concentrations. The total amount of SO_4^{2-} in solution was held constant from preparation to preparation, however, by increasing the volume of soaking solution. The sulfate concentrations of three of the samples prepared in this way, in soaking solutions of pH 0.0, 1.2, and 8.2, were measured by inductively coupled plasma (ICP) analysis after calcination. We have found that the sulfur loadings for these three samples were between 6–7% by weight in the form of SO_3.

The pH was measured with a calibrated Corning 355 model pH/ion analyzer equipped with an Accumet gel-filled electrode, referenced to a calomel electrode. The mixture of support and pH adjusted soaking solution was stirred for 2 h. The samples were then filtered, dried in an oven at 120°C for 12 h, and vacuum dried for 8 h at 120°C, as above. Samples were prepared for pH values of 1.2, 6.6, 8.8, and 9.7. The absence of samples between pH values of 2 and 6 is explained by the difficulty of preparing soaking solutions with pH values near the equivalence point of the titration curve, which lies within this region.

All catalysts were activated by heating at 600°C for 1 h under vacuum conditions, and then analyzed by powder X-ray diffraction (XRD) to confirm the formation of the crystalline zirconia tetragonal phase. The activated samples were stored in a Vacuum Atmospheres N_2/Ar atmosphere glove box until used.

Deuterium-exchanged sulfate-promoted zirconium oxide catalyst was prepared according to the procedure mentioned above except deuterium oxide (2ml, Aldrich NMR grade) was introduced via vacuum line transfer after the activation step and then heated at 120°C for 12 h. The excess ^2H_2O was removed by vacuum.

Catalyst Analysis

Thermogravimetric analysis (TGA) and differential thermal analysis (DTA) experiments were performed on a Seiko TG/DTA SSC15200 instrument under argon gas purge at a flow rate of 120 ml/min. Samples, typically consisting of 30–50 mg of material, were heated to 1000°C at a rate of 5°C/min in platinum crucibles. α-Al_2O_3 was used

as a mass reference. Powder XRD measurements were performed at the PNNL X-ray crystallography facility on a diffractometer consisting of two Philips wide-range vertical goniometers with incident-beam 2-theta compensating slits, integral soller slits, fixed receiving slits, diffracted beam graphite monochromators, and scintillation counter detectors. The X-ray source was a Philips XRG3100 X-ray generator with a fixed anode, long-fine-focus Cu tube at 1800 W.

Sulfur and zirconium content for the sulfate-promoted samples was measured by inductively coupled plasma (ICP) chemical analysis. Surface areas were measured using the BET method (41) on a Quantachrome surface area analyzer. The results reported here are the average of three measurements, with a spread of no more than ± 2 m^2/g. Samples were degassed and heated at 120°C for 1 h prior to adsorption measurements. Infrared spectroscopy experiments were performed on a Nicolet Magna-IR 750 spectrometer. Powdered specimens were diluted with KBr (Aldrich IR grade) to 1% dilution in order to avoid opacity at low wavenumber values and the sample chamber purged with N_2 gas before data acquisition. A pellet of pure KBr was scanned for a background signal.

Activity Determination

Uncalcined material (750 mg) was placed in a quartz reactor tube (ID = 4 mm) positioned in the center of a jacket furnace. The sample was activated by heating for 1 h at 600°C in a flowing nitrogen atmosphere and then cooled to 220°C. The n-butane feed gas (8% n-C_4H_{10}/92% He) was introduced through an inlet valve (at flow rates of $3.8 \times 10^{-4} \pm 0.5 \times 10^{-4}$ liter s^{-1}) attached to a pressure gauge. Gas samples were periodically extracted by syringe from an outlet sample port positioned after the catalyst bed. The extracted samples were injected into a Hewlett–Packard 5890 gas chromatography (GC) system for analysis. The fraction of isobutane in the product gas was expressed as a percent selectivity, defined as

$$\%\ \text{selectivity} = 100\% \times \frac{4[\text{i-C}_4]}{4[\text{i-C}_4] + 3[\text{C}_3] + 5[\text{C}_5]}. \quad [1]$$

The percentage yield of isobutane was defined in the usual way as

$$\%\ \text{yield} = 100\% \times \frac{4[\text{i-C}_4]}{4[\text{n-C}_4] + 4[\text{i-C}_4] + 3[\text{C}_3] + 5[\text{C}_5]}. \quad [2]$$

Activity was defined as the rate of n-butane conversion per gram of catalyst,

$$\text{Activity} = \frac{\text{FP}}{\text{W}_\text{c}\text{RT}} \times \frac{4[\text{i-C}_4] + 3[\text{C}_3] + 5[\text{C}_5]}{4[\text{n-C}_4] + 4[\text{i-C}_4] + 3[\text{C}_3] + 5[\text{C}_5]}, \quad [3]$$

where F is the input gas flow rate, P is atmospheric pressure, W_c is the mass of the catalyst, and $[C_n]$ are the relative concentrations of the alkanes derived from the GC measurements, taken at the outlet of the reactor.

^1H NMR Spectroscopy

Variable temperature proton NMR measurements were performed on a Varian Unity*plus* console equipped with a 11.7 Tesla Oxford Instruments magnet. A Doty Scientific 5-mm CRAMPS probe with silicon nitride rotors and Kel-F end caps was used. The rotors were packed in a N_2/Ar atmosphere. 1.5 μs 90° pulse widths and 5–60 s delays between scans were typical parameters, depending on the sample and temperature.

Up to 20–30% of the detected proton NMR signal originated from sources other than the sample, primarily the probe. For single-pulse experiments, the background signal was eliminated by performing experiments twice, once with a sample and once without, and subtracting free induction decays.

NMR relaxation times were determined by monitoring the recovery of the magnetization after saturation (42). This approach was especially advantageous at low temperatures where T_1 values were long. Twenty to thirty 90° pulses separated by 5 μs sufficed to assure complete saturation.

Proton CRAMPS spectra of the zirconia samples were recorded on a Varian Unity*plus* spectrometer equipped with a 7.1 Tesla Oxford Instruments magnet and a Varian 5-mm CRAMPS probe. Standard multiple pulse tune-up procedures (43) were carried out with a 5-mm glass bulb of liquid benzene doped with chromium(III) acetylacetonate. We have used two multiple-pulse sequences, MREV-8 (44) and BR-24 (45), in these experiments, but observed little difference in resolution between the two. In this paper, we report only the MREV-8 results. A phase-cycle was employed to double the spectral width of the experiment and optimize signal intensity (46). NMR parameters for multiple pulse experiments were 90° pulse widths between 1.5 μs, 512 complex data points acquired, and delays between scans of 5–100 s, depending on sample and experiment temperature. A cycle time for the MREV-8 sequence was typically 42 μs. The CRAMPS spectra were referenced to an external ^1H chemical shift standard of solid tris (trimethylsilyl)-silane (TTMS).

Simulations

Spectra were simulated for comparison with the experimental data by calculating the FID using a density matrix approach (47),

$$S(t) = \langle \text{Tr}\{DU\rho_o U^\dagger\}\rangle, \quad [4]$$

where S(t) is the amplitude of the FID at time t, U and $U^\dagger$ are the unitary time development operator and its inverse,

respectively, ρ_o is the initial density matrix, and D is the detection operator,

$$D = \sum_j I_+^j. \quad [5]$$

The summation in [5] is performed over all coupled protons. The brackets signify that a powder average was performed. The time development operators were derived from the total Hamiltonian,

$$\mathcal{H}_T = \sum_j \left[\mathcal{H}_{CSA}^j + \sum_{i,j\neq i} (1/2)\mathcal{H}_{d-d}^j \right], \quad [6]$$

where $\mathcal{H}_{CSA}^j$ is the Hamiltonian describing the chemical shift anisotropy (CSA) for spin i,

$$\mathcal{H}_{CSA}^j = \mathbf{I}^j \sigma_j, \quad [7]$$

and $\mathcal{H}_{d-d}^j$ is the usual homonuclear dipolar interaction Hamiltonian (47).

All calculations were performed on a SGI Onyx computer. The simulation programs we have developed incorporate C++ modules created by Smith *et al.* (48).

RESULTS AND DISCUSSION

TGA and IR

Table 1 lists the surface area and percentage of weight loss in the temperature range 500–1000°C from TGA for zirconium oxide, sulfate-promoted zirconium oxide, and modified sulfate-promoted zirconium oxide samples. Surface areas for all samples dried at 120°C average 200 ± 20 m^2/g, and decrease significantly after calcining at 600°C to 50 ± 30 m^2/g as a result of the transition of the amorphous support to the tetragonal phase of ZrO_2 ($T_c \sim 475$°C (18)). Weight loss in this temperature range is due primarily to the removal of both adsorbed sulfate (in the form of SO_3) and physisorbed water at lower temperatures. The TGA data in Fig. 1 show that the weight loss of samples dried at 120°C is greater than for those dried at 600°C, as expected, and some adsorbates remain on the catalyst even after calcining at 600°C under vacuum conditions. For unpromoted zirconium hydroxide, the removal of adsorbates appears to be complete at 500°C with very little difference in weight loss between samples prepared at 120°C and 600°C. Comparing the percentage of weight loss for the modified samples after calcining at 600°C, it appears that, as the pH increases, the total amount of removable adsorbates decreases.

TABLE 1

Selected Properties of the Zirconium Oxide and Sulfate-Promoted Zirconium Oxide Samples Studied

Sample (calc. temperature)	Surface area (m^2/g)	Percentage of weight loss[a] (from TGA)
$Zr(OH)_4$ (120°C)	194.6	1.8
ZrO_2 (600°C)	8.99	1.0
SO_4/ZrO_2 (120°C)	205.3	10.6
SO_4/ZrO_2 (600°C)	10.7	3.0
SO_4/ZrO_2 pH 1.2 (120°C)	210.8	13.9
SO_4/ZrO_2 pH 1.2 (600°C)	32.9	3.0
SO_4/ZrO_2 pH 6.6 (120°C)	215.8	
SO_4/ZrO_2 pH 6.6 (600°C)	97.3	1.5
SO_4/ZrO_2 pH 8.8 (120°C)	189.0	5.8
SO_4/ZrO_2 pH 8.8 (600°C)	41.03	0.6
SO_4/ZrO_2 pH 9.7 (120°C)	225.1	
SO_4/ZrO_2 pH 9.7 (600°C)	73.2	0.3

Note. The pH of the sulfating solutions were adjusted by titrating with 1 *M* NH_4OH solution (see text).

[a] Values from 500°C ≤ T ≤ 1000°C.

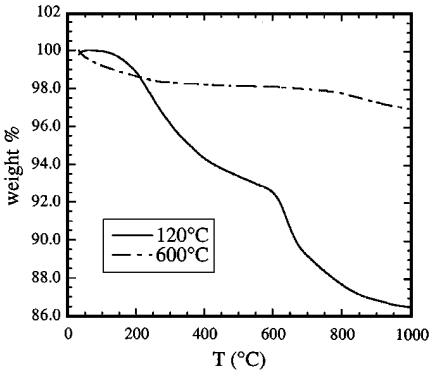

FIG. 1. Weight loss as a function of temperature of SO_4/ZrO_2 catalyst calcined at 120 and 600°C.

Figure 2 shows IR spectra for modified and unmodified sulfate-promoted zirconium oxide catalysts calcined at 600°C. All spectra contain peaks in the regions characteristic of hydroxyl stretching (3400 and 3100 cm^{-1}) and water bending (1600 cm^{-1}) modes. Based on previous assignments (22, 23) the broad peak between 3500 and 3200 cm^{-1} is attributed to hydrogen-bonded hydroxyl groups and physisorbed water, while the broad peak between 3200 and 2900 cm^{-1} can be assigned to hydroxyl stretches perturbed by neighboring sulfate groups. The sulfate stretching region is observed between 1300 and 900 cm^{-1} and shows a broad absorbance line with shoulders at ~1280, ~1150, and ~1050 cm^{-1}. This type of SO_4 stretching pattern is typical of sulfato complexes in a bidentate configuration (17). Although the concentration of both hydroxyl groups and physisorbed water decreases upon increased drying temperature, heating the catalyst to 600°C does not completely deprotonate the surface, an observation in agreement with the TGA results.

The absorbance intensity in the 3600–3000 cm^{-1} region, corresponding to the hydroxyl stretching region, is greater for the unmodified sample (pH ~0) than for the samples prepared at higher pH values. The largest change is

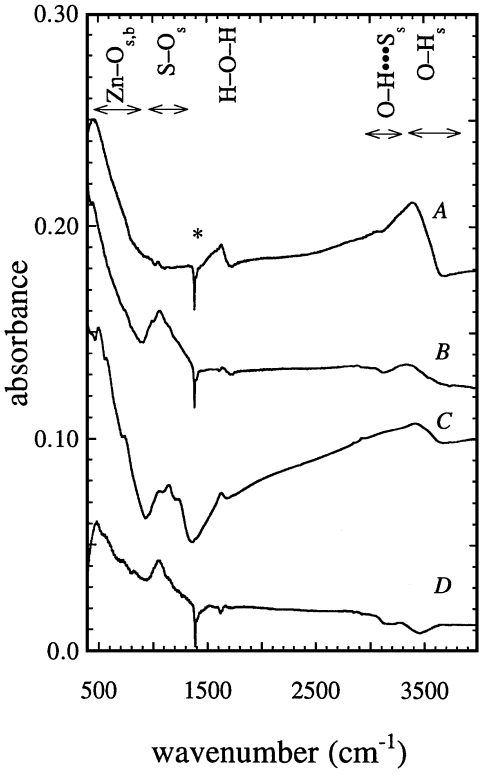

FIG. 2. Infrared spectroscopy experiments of SO_4/ZrO_2 catalysts prepared in pH 0 (A), 1.2 (B), 6.6 (C), and 9.7 (D) sulfating solutions. All samples were calcined at 600°C for 1 h. Assignment of absorbances are noted. The sharp negative peak at ~1390 cm^{-1} is a KBr absorbance. The spectra have been shifted vertically to improve visibility.

observed in comparing the unmodified sample to the pH 1.2 sample. A slight change in absorbance intensity is observed comparing the pH 1.2 to pH 6.6 samples. At pH 9.7, the number of protonated sites remaining on the catalyst is greatly decreased, compared to a sample prepared at pH 0, as shown by the diminished intensity in the 3400 cm^{-1} region.

We have also examined an unmodified sulfate-promoted zirconium oxide catalyst that has been reacted with deuterium oxide after calcining at 600°C. The IR results show a new peak at ~2550 cm^{-1}, which is indicative of an O-D stretching mode. The observation of an O-D stretch demonstrates that a portion of the proton population is exchangeable, and thus ostensibly near the surface.

Catalytic Activity Testing

Figure 3 contains plots of the percentage selectivity as a function of time on-stream. For all samples, the initial percentage selectivity was found to be in the range 70–80% and increased to asymptotic values in the range of 80–95% after about 15 min. The percentage yield is shown in Fig. 4A and is characterized by a high initial activity followed by an exponential decay. Steady state yields were extracted from the single exponential fits of the percentage yield data. Figure 4B shows a plot of the steady state yield versus soaking solution pH for the different catalysts.

Plots of activity as a function of time on-stream for the reaction n-butane to iso-butane at 220°C for both unmodified and pH-modified sulfate-promoted zirconium oxide samples are shown in Fig. 5. In general, the activity starts at 40–500 nmol cm s^{-1} g^{-1} and decreases approximately exponentially. The activities measured here are consistent with activities measured elsewere (9, 31–33), taking into account the differences in calcination temperature and atmosphere and reaction conditions. The decrease in activity over time is due, at least in part, to the formation of coke (31), the reduction of sulfur at the active sites (49, 50), and loss of water or hydroxyl groups at the surface (31). Catalytic activity could be restored by recalcining at 600°C. The activity data could be fitted to a double exponential model assuming high initial activity followed by a lower, longer-lived activity, as reported by Yaluris *et al.* (31).

The presence of NH_3 has been shown to poison the active sites of ZrO/SO_4 catalysts (31, 32). However, the presence of ammonium hydroxide used in the soaking solution in this study does not appear to affect the catalytic performance of the samples. There is no evidence of distinctive NH symmetric or asymmetric stretching modes (3450–3200 cm^{-1}) or NH_2 deformation (scissors) vibrations (850–750 cm^{-1}) in the IR spectra for either samples that have been dried

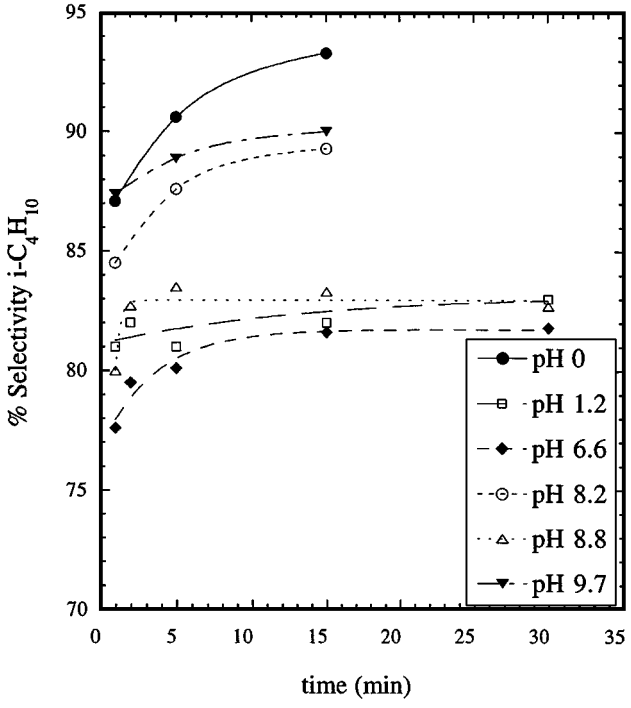

FIG. 3. Percentage selectivity of SO_4/ZrO_2 catalysts prepared in soaking solutions of varying pH as a function of time on stream for the isomerization of n-butane to isobutane at 220°C.

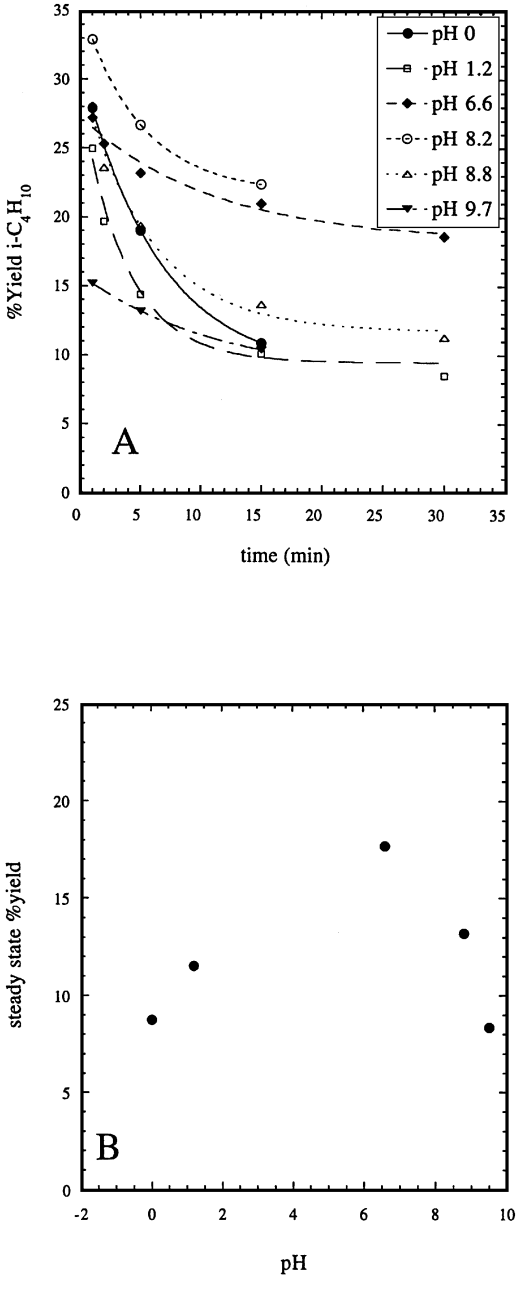

FIG. 4. Percentage yield as a function of time on stream (A) and steady state yield as a function of sulfating solution pH (B) of SO_4/ZrO_2 catalysts prepared in soaking solutions of varying pH for the isomerization of n-butane to iso-butane at 220°C.

at 120°C or calcined at 600°C. Amine-containing species are also absent, as determined by ICP. We conclude that the washing of the catalyst was sufficient to remove any ammonium species present. Even though no NH adsorbances (1600–1400 cm^{-1}) are seen in any of the IR spectra, an ammonium hydroxide promoted sample was also tested for activity to verify that surface adsorbed ammonium was not associated with the catalytic activity. No sign of catalytic activity was observed. Samples prepared by titrating the sulfate soaking solution with 1 *M* NaOH instead of 1 *M* NH_4OH were also tested for catalytic activity for the isomerization of n-butane to iso-butane at 220°C. These samples were not active. Although alkali metals have been used as promoters for some catalytic reactions, they are known to poison some catalytic surfaces (51).

The IR and TGA data show that for the samples prepared at pH values between pH 0–8.8, there are protonated sites on the catalyst after activation at 600°C and that the concentration of these sites is dependent on the pH of the sulfating solution. As the data in Table 1 illustrate, the BET surface area of the sulfate-promoted samples appears to be a sensitive function of the soaking solution pH, with the surface area reaching a maximum for samples prepared in soaking solutions with pH values between 6.6 and 8.8. Assuming the surface density of active sites is the same for each of these samples, one might expect that samples with the highest surface area would also be the samples most effective at catalyzing the n-butane to isobutane isomerization reaction. Indeed, we find that it is the samples with the largest surface areas that have the highest activities and yields of the sulfate-promoted zirconias synthesized in this study, suggesting that the activity dependence on pH is at least partly explained as a surface area effect, with preparation conditions, such as pH, that maximize surface area leading to catalysts with optimized activity.

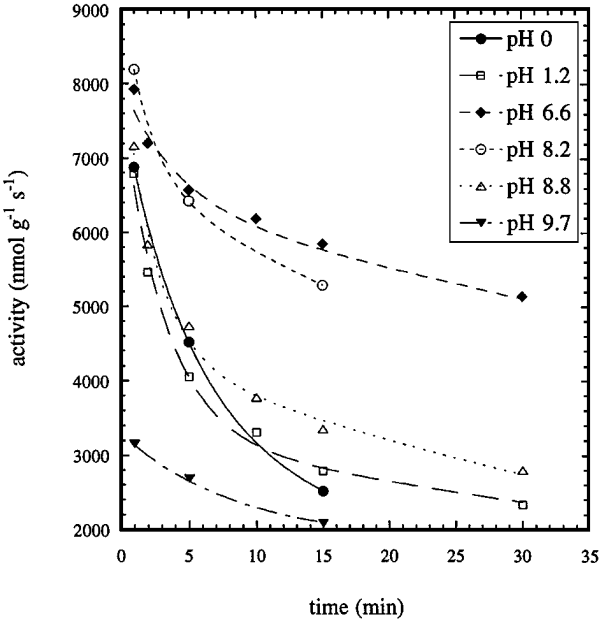

FIG. 5. Catalytic activity versus time on stream for the isomerization of n-butane to iso-butane at 220°C. The curves represent two-exponential fits to the data representing an initial high activity and a smaller long time activity (see text).

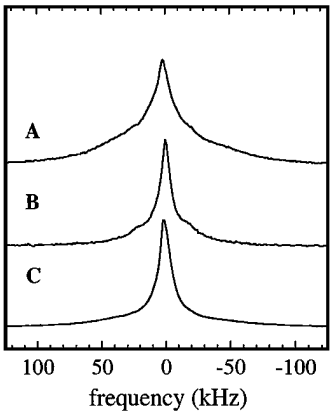

FIG. 6. ^{1}H NMR of (A) NH_4OH adjusted SO_4/ ZrO_2, (B) SO_4/ZrO_2, and (C) ZrO_2 heated at 600°C.

NMR

Low temperature ^{1}H NMR spectra of sulfate-promoted zirconium oxide catalysts calcined at 600°C are shown in Fig. 6. Spectra for the modified and unmodified samples are similar in that the lineshapes were found to be composed of a sharp narrow central component with broad shoulders at ±20 kHz. The spectrum from the untreated zirconia support, however, is not comparable in complexity, even at temperatures as low as −120°C. Based on the linewidths of the ^{1}H NMR resonances and low paramagnetic concentrations, it is evident that strong homonuclear dipolar couplings dominate the NMR spectra and conceal the proton chemical shifts.

CRAMPS ^{1}H chemical shift spectra are shown in Fig. 7. The sharp, negative peaks near 0 ppm are carrier frequency artifacts arising from imperfections of the phase cycle (46). All other resonances are reported in Table 2. Three resonances are identified: 6.7 ± 0.3, 3.0 ± 1.0, and 0.0 ± 0.5 ppm. Based on previous ^{1}H NMR work on dehydrated surfaces (52–54) and theoretical calculations (55) these resonances can be assigned to acidic hydroxyl groups, physisorbed molecular water molecules, and isolated, non-hydrogen bonded hydroxyl groups, respectively.

TABLE 2

Isotropic Chemical Shifts Measured for Modified and Unmodified Sulfate Promoted Zirconium Oxide Catalysts Using CRAMPS

Sample (pH/calc. T°C)	∂_{iso} (±1 ppm)	∂_{iso} lit. (ref.)
SO_4/ZrO_2 (0/600°C)	6.8, 3.3, 0.0	6, ~2 (6, 9); 8.4, 6.3, 1.3 (35)
SO_4/ZrO_2 (8.8/600°C)	6.3, 3.0, 0.0	
ZrO_2 (na/600°C)	6.0, 2.2, 0.0	4.5, 1.7 (9) 3.86, 1.6 (6)

The primary difference between the catalytically active samples and the unpromoted support is the shift to lower shielding of the prominent middle resonance observed for the sulfated samples.

The values for the chemical shifts found here are slightly different from those reported on the basis of MAS alone, particularly for the more acidic sites. The large linewidths reflect a distribution of isotropic chemical shifts, and are not due to imperfections in the MAS or CRAMPS experiments. Motion can also reduce the line-narrowing effectiveness of MAS and CRAMPS experiments (52–54), especially when the correlation times of the motion are similar to the rotor periods or cycle time of the multiple pulse experiment.

The saturation recovery curve measured at −120°C for the sulfate-promoted zirconium oxide sample calcined at 600°C is displayed in Fig. 8, along with nonlinear least squares one- and two-exponential fits. Although the two-exponential equation has more degrees of freedom, reduced chi-squared comparisons of the two fits indicate that

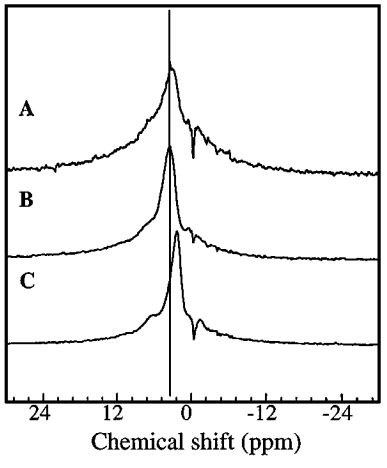

FIG. 7. 300 MHz ^{1}H CRAMPS spectra of (A) SO_4/ZrO_2, (B) NH_4OH adjusted SO_4/ZrO_2, and (C) ZrO_2. All samples were calcined at 600°C for 1 h.

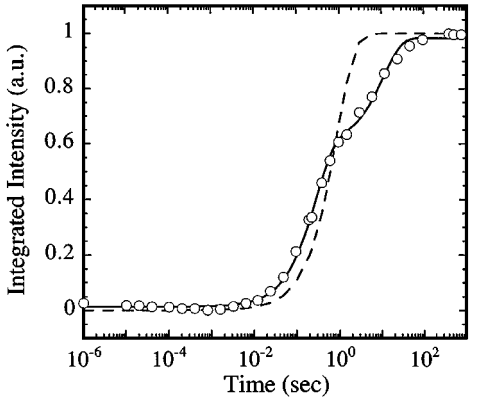

FIG. 8. NMR intensity vs logarithm of the saturation recovery time, recorded at −120°C with a one (dashed line) and two exponential fit (solid line) for NH_4OH-modified ZrO_2/SO_4^{2-} at pH 8.8, calc. 600°C.

the superiority of the two-exponential model is statistically meaningful. The best-fit spin-lattice relaxation times for the two-exponential curve at −120°C are 200 ms and 6 s.

The large disparity in relaxation times can be used to separate the signal of the magnetization recovering with a short T_1 from the signal of the magnetization recovering with a long T_1. This is accomplished in the following way. According to the two-exponential model used to fit the saturation recovery data, the normalized amplitude of the NMR signal after a saturation recovery time t can be written

$$A(t) = 1 - A_S e^{-t/T_{1,S}} - A_L e^{-t/T_{1,L}}, \quad [8]$$

where A_S and A_L are the relative fractions ($A_S + A_L = 1$) and $T_{1,S}$ and $T_{1,L}$ are the relaxation times of the short and long T_1 components, respectively. If $T_{1,S}$ and $T_{1,L}$ differ by a factor of 10 or more, then an intermediate recovery time t_I can be selected, where

$$A(t_I) \approx A_s. \quad [9]$$

In Fig. 8, this time corresponds to the "knee" in the curve around $t \approx 1$ s. This is the interval where the magnetization associated with the $T_{1,S}$ relaxation time has fully recovered and the magnetization associated with the $T_{1,L}$ relaxation time remains fully saturated. A spectrum measured at this value of t contains only the signal from magnetization associated with the $T_{1,S}$ relaxation time. The spectrum of the magnetization associated with the $T_{1,L}$ relaxation time can be obtained from this signal and the signal measured at long t ($t \gg T_{1,L}$) by subtracting one FID from the other.

Figure 9 reveals that the long and short T_1 components have distinctly different spectra, the short T_1 component having a broad lineshape sensitive to temperature and the long T_1 component having a triplet-like line shape that is less sensitive to temperature. The temperature dependence of the lineshape suggests that the protons are not fixed on the time scale of the NMR measurement. At higher temperatures (120 and 25°C), the lineshape of the short T_1 component resembled a single Gaussian with a linewidth of 15 kHz with a faint shoulder at 24 kHz. Lowering the sample temperature to −120°C results in an extremely broad NMR signal with a linewidth of over 60 kHz.

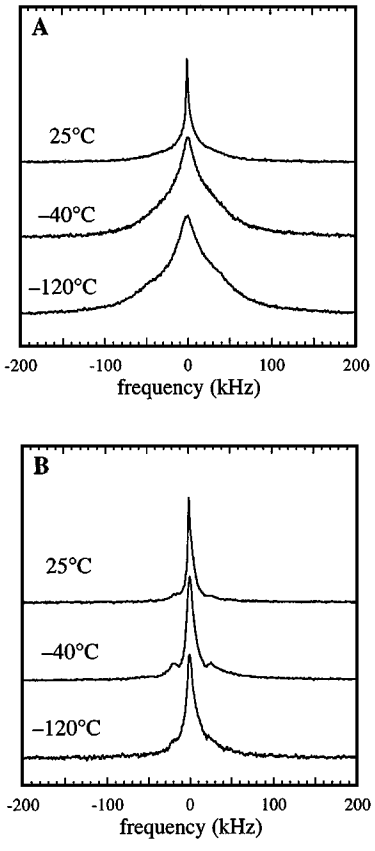

FIG. 9. Variable temperature ^{1}H NMR of NH_4OH modified ZrO_2/SO_4^{2-} at pH 8.8, calc. 600°C, (A) the short T_1 component and (B) the long T_1 component.

The long T_1 component at 120°C consists of a single peak with a linewidth of approximately 20 kHz. At 25°C, shoulders appear at ±20 kHz. Finally, at a temperature of −120°C, the resonance broadens and the shoulders become increasingly prominent. However, the lineshape ceased changing at temperatures near −30–40°C, implying the cessation of motion. Similar findings have been shown for the surfaces of γ-Al_2O_3 (56) and silicas (52–54), where the mobile species was migrating hydroxyl groups. Proton motion with correlation times of $t_c \sim 100$ ms have previously been observed in other studies of hydrated metal oxide surfaces (52–54, 56).

Although the lineshapes of these spectra remained constant below −40°C, the T_1 relaxation rate for both components continues to increase as the temperature decreased, as shown in Fig. 10A. A plot of the fractional populations of the two proton species versus temperature, shown in Fig. 10B, illustrates the finding that the population

TABLE 3

Summary of Proton Position Used to Calculate ^{1}H NMR Spectral Simulations Perfomed for SO_4/ZrO_2

Position	x (Å)	y (Å)	z (Å)
1a	1.20	1.67	2.82
1b	2.14	1.67	2.82
2	0.00	0.81	0.58
3	0.00	−0.81	0.58
4	0.86	−1.67	0.58
5	2.48	−1.67	0.58
6	3.33	0.81	0.58
7	3.33	−0.81	0.58

Note. A diagram of the proton positions is shown in Fig. 11. Sample simulations are shown in Fig. 12. All simulations consisted of four protons; see text.

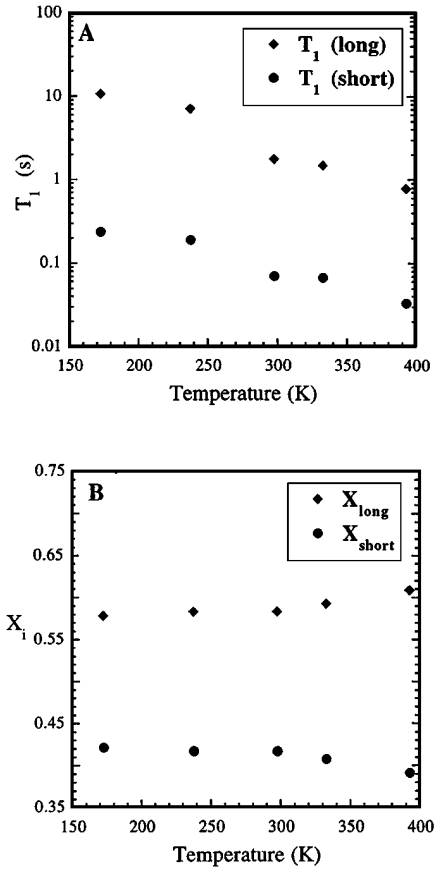

FIG. 10. (A) log of spin-lattice relaxation time (T_1) versus temperature and (B) percentage of population versus temperature for the two relaxation components on sulfate-promoted zirconium oxide for NH_4OH modified ZrO_2/SO_4^{2-} at pH 8.8, calc. 600°C.

of each component did not change throughout the temperature range. This constancy would be improbable if the two-population model were an artifact of the fitting procedure.

One possible identity for the long T_1 population is protons associated with the sulfate group or surface hydroxyl groups lying in close proximity to surface water protons. Both hydroxyl groups and water are known to be present by IR spectroscopy for samples calcined at temperatures as high as 600°C. Theoretical spectra based on this assumption were calculated using Eqs. [4]–[7] for comparison with the experimental low temperature ^{1}H NMR spectra. The protons were assumed to be fixed on the time scale of the NMR measurement (see above). Atomic coordinates were calculated by simulating the 110 face of the tetragonal phase of ZrO_2 (57) with slight local structural distortions due to the presence of a bridging sulfate group. Proton positions were assumed to be at four of the possible eight sites considered and shown in Fig. 11 and listed explicitly in Table 3. Twenty-four structural models were chosen and are listed in Table 4. Eight of these structural models contain a water molecule situated at proton sites 2 and 3, with an interproton separation of 1.54 ± 0.02 Å. The additional 16 models consist only of isolated hydroxyl groups. An additional model consisting of an isolated hydronium ion arranged as an isosceles triangle with an interproton distance of 1.58 Å was also considered. To account for the slight asymmetry of the experimental spectrum, we have found it necessary to assume an axially symmetric chemical shift anisotropy interaction for the protons on the water molecule, but we have not included the CSA terms for the hydroxyl protons due to the many extra degrees of freedom introduced by these anisotropic tensorial interactions.

Results of these simulations are shown in Fig. 12A. Four classes of spectra were obtained with the following features: (1) a broad central feature with shoulders at ~±50 kHz, (2) a broad central feature with shoulders at ~±20 kHz, (3) a broad Gaussian resonance, and (4) a broad central feature with symmetric shoulders at ~±50 kHz. Specific intensities of the shoulders or linewidths varied for simulations within each class to within ±10%, depending on the structural model used. The class 1 and 2 simulations incorporate discrete water molecules while the class 3 and 4 models are without water molecules. The class 1 and 4 models have protons in closely neighboring, electrostatically unfavorable positions (sites 3 and 4, for example), with proton–proton distances of ~1.2 Å. The class 3 configurations consist only of weakly coupled hydroxyl groups. The class 2 models contain a water molecule interacting with two distant (>2 Å) protons, and produce the best agreement with the experimental data. Refinement of the shoulder splitting and intensities, by adjusting the proton internuclear distance in the H_2O molecule and the asymmetry of

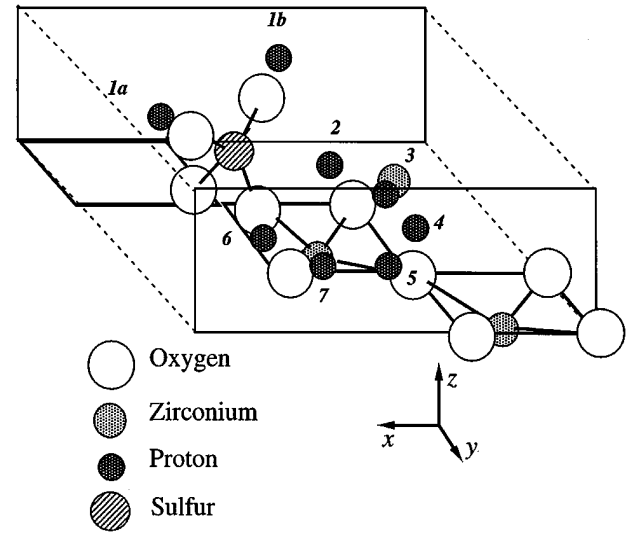

FIG. 11. Structural model used for the simulation of ^{1}H NMR lineshapes. Based on the 110 face of tetragonal ZrO_2 (57) and the surface model proposed by Clearfield *et al.* (40).

TABLE 4

Summary of ^{1}H NMR Spectral Simulations Performed for SO_4/ZrO_2

Simulation #	Sites	H_2O?	CSA of H_2O (kHz)	Spectrum class
1	1a, 2, 3, 4	yes	9.5	1
2	1a, 2, 3, 5	yes	9.5	2
3	1a, 2, 3, 6	yes	9.5	2
4	1a, 2, 3, 7	yes	9.5	2
5	1b, 2, 3, 4	yes	9.5	1
6	1b, 2, 3, 5	yes	9.5	2
7	1b, 2, 3, 6	yes	9.5	2
8	1b, 2, 3, 7	yes	9.5	2
9	1a, 2, 4, 6	no	n/a	3
10	1a, 2, 4, 7	no	n/a	3
11	1a, 3, 4, 6	no	n/a	4
12	1a, 3, 4, 7	no	n/a	4
13	1a, 2, 5, 6	no	n/a	3
14	1a, 2, 5, 7	no	n/a	4
15	1a, 3, 5, 6	no	n/a	3
16	1a, 3, 5, 7	no	n/a	4
17	1b, 2, 4, 6	no	n/a	3
18	1b, 2, 4, 7	no	n/a	3
19	1b, 3, 4, 6	no	n/a	4
20	1b, 3, 4, 7	no	n/a	4
21	1b, 2, 5, 6	no	n/a	3
22	1b, 2, 5, 7	no	n/a	4
23	1b, 3, 5, 6	no	n/a	3
24	1b, 3, 5, 7	no	n/a	4

Note. Proton positions are listed in Table 3 and are shown in Fig. 11. All simulations consisted of four protons; see text.

the CSA tensor, resulted in the following parameters corresponding to the best fit shown in Fig. 12B: $r_{2,3} = 1.52$ Å, $\sigma_{xx} = \sigma_{yy} = 0.0$, $\sigma_{zz} = -19.0$ ppm. This corresponds to simulation model 4 in Table 4.

Despite the good agreement between the simulations and the experimental spectra, the four-proton site model we have proposed should be considered as only an idealized model of the more complicated situation that exists on the zirconia surface. Numerous plausible structural moieties could exist at the surface, including sites similar to the models that result in simulations of class 1, 3, and 4. It is more realistic to assume that the observed spectra are a weighted average of spectra from a number of related sites. The experimental spectra also vary from sample to sample in intensity and asymmetry of the shoulders. The idealization notwithstanding, the following conclusions can be inferred regarding the arrangement of protons on the surface: (1) the sites corresponding to the long T_1 spectrum contain discrete water molecules near sulfate sites, and (2) neither hydronium ions or isolated hydroxyl groups are present in the long T_1 component spins. The large splittings (on the order of 20 kHz) observed in the NMR spectra imply the existence of static, closely-spaced protons as occur, e.g., in crystalline water molecules (58). The weaker homonuclear dipolar couplings of random, isolated hydroxyl groups could not plausibly account for the experimental spectra. Hydronium ions may be dissociating to form weakly coordinated H_2O–H species with the third proton hydrogen-bonded to a neighboring oxygen.

The multi-component ^{1}H NMR lineshape is thus explained by a surface model consisting of isolated proton arrangements similar to the water-sulfate structure shown in Fig. 11 surrounded by abundant surface hydroxyl groups. This arrangement of protons is consistent with a model containing Brønsted and Lewis acid sites proposed by Clearfield *et al.* (40), modified by the addition of a water molecule. While the variable temperature NMR results indicate that water or hydroxyl groups are mobile on the surface at temperatures above −100°C, at lower temperatures the hydrogenated sites are sufficiently slowed to be captured on NMR time scales. The model depicted in Fig. 11 thus is best considered as a "snapshot" of the presumptive active site on a dynamic surface.

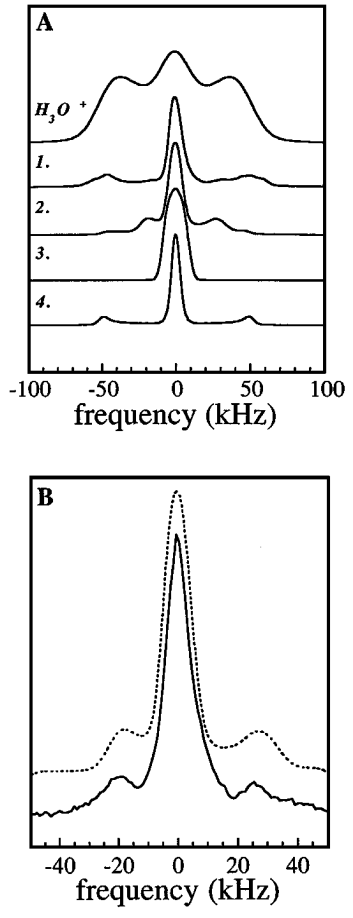

FIG. 12. Simulation of ^{1}H NMR lineshape using models tabulated in Table 4 based on structural model depicted in Fig. 11. (A) Depiction of four classes of simulations and simulation of hydronium ion. (B) Best fit (dashed line) derived from model four and experimental data (solid line) for NH_4OH modified ZrO_2/SO_4^{2-} at pH 8.8, −40°C.

ACKNOWLEDGMENT

We thank P. D. Ellis for valuable discussions and acknowledge the assistance of D. McCready (powder X-ray diffraction measurements), G. Roberts (activity measurements), and R. Sell and R. Scheele (thermal analysis). RSM was supported by an appointment to the Distinguished Postdoctoral Research Program sponsored by the U.S. Department of Energy Office of Education Programs and administered by the Oak Ridge Institute for Science and Education, and DFS was supported by the Associated Western Universities, Inc., Northwest Division, under Grant DE-FG06-89ER-7522. The Pacific Northwest National Laboratory is operated for the U.S. Department of Energy by the Battelle Memorial Institute under Contract DE-AC06-76RLO-1830.

REFERENCES

1. Melchor, A., Garbowski, E., Mathieu, M. V., and Primet, M., *J. Chem. Soc. Faraday Trans.* **82**, 1893 (1986).
2. Hino, H., Kobayashi, S., and Arata, K., *J. Am. Chem. Soc.* **101**, 6439 (1979).
3. Hino, H., and Arata, K., *J. Chem. Soc. Chem. Commun.* 851, 1980.
4. Arata, K., Hino, M., and Yamagata, N., *Bull. Chem. Soc. Jpn.* **63**, 244 (1990).
5. Chen, F. R., Coudurier, G., Joly, J-F., and Vedrine, J. C., *J. Catal.* **143**, 616 (1993).
6. Riemer, T., Spielbaker, D., Hunger, M., Mekhemer, C. A. H., and Knozinger, H., *J. Chem. Soc., Chem. Commum.* 1181, 1994.
7. Lin, C. H., and Hsu, C. Y., *J. Chem. Soc. Chem. Commun.* 1479, 1992.
8. Garin, F., Seyfried, L., Girard, P., Maire, G. Abdulsamad, A., and Sommer, J., *J. Catal.* **151**, 26 (1995).
9. Adeeva, V., de Haan, J. W., Janchen, J., Lei, G. D., Schunemann, V., van de Ven, L. J. M., Sachtler, W. M. H., and van Santen, R. A., *J. Catal.* **151**, 364 (1995).
10. Komarov, V. S., and Sinilo, M. F., *Kinet. Katal.* **29**, 605 (1988).
11. Nitta, M., Sakoh, H., and Aomura, K., *Appl. Cat.* **10**, 215 (1984).
12. Nascimento, P., Akratopoulou, C., Oszagyan, M., Coudurier, G., Travers, C., Joly, J. F., and Vedrine, J. C., *in* "Proceedings, 10th International Congress on Catalysis, Budapest, 1992," Paper O 80.
13. Jin, T., Yamaguchi, T., and Tanabe, K., *J. Phys. Chem.* **90**, 4794 (1986).
14. Bensitel, M., Saur, O., Lavelley, J. C., and Mabilon, G., *Mater. Chem. Phys.* **17**, 249 (1987).
15. Morterra, C., Cerrato, G., Pinna, F., and Signoretto, M., *J. Catal.* **157**, 109 (1995).
16. Morterra, C., Cerrato, G., Emanual, C., and Bolis, V., *J. Catal.* **142**, 349 (1993).
17. Morterra, C., Cerrato, G., Pinna, F., Signoretto, M., and Strukul, G., *J. Catal.* **149**, 181 (1994).
18. Srinivasan, R., Keogh, R. A., Milburn, D. R., and Davis, B. H., *J. Catal.* **153**, 123 (1995).
19. Srinivasan, R., Keogh, R. A., and Davis, B. H., *Catal. Lett.* **36**, 51 (1996).
20. Riemer, T., and Knozinger, H., *J. Phys. Chem.* **100**, 6739 (1996).
21. Babou, F., Coudurier, G., and Vedrine, J. C., *J. Catal.* **152**, 341 (1995).
22. Kustov, L. M., Kazansky, V. B., Figueras, F., and Tichit, D., *J. Catal.* **150**, 143 (1994).
23. Platero, E. E., and Montruit, M. P., *Catal. Lett.* **30**, 31 (1995).
24. Morterra, C., Aschieri, R., and Volante, M., *Mater. Chem. Phys.* **20**, 539 (1988).
25. Bensitel, M., Saur, O., Lavalley, J. C., and Morrow, B. A., *Mater. Chem. Phys.* **19**, 147 (1988).
26. Sharygin, L. M., Denisova, S. M., Vovk, S. M., Perekhozheva, T. N., Pletnev, R. N., and Gonchar, V. F., *Zh. Neorg. Khim* **30**(8), 1968 (1985).
27. Parshutkin, V. V., Yaroslavtsev, A. A., Prozorovskaya, Z. N., and Mun, A. I., *Zh. Neorg. Khim* **30**(1), 56 (1985).
28. Egashira, M., Nakashima, M., Kawasumi, S., and Selyama, T., *J. Phys. Chem.* **85**, 4125 (1981).
29. Gercher, V. A., and Cox, D. F., *Surf. Sci.* **322**, 177 (1995).
30. Goniakowski, J., and Gillan, M. J., *Surf. Sci.* **350**, 145 (1996).
31. Yaluris, G., Larson, R. B., Kobe, J. M., Gonzales, M. R., Fogash, K. B., and Dumesic, J. A., *J. Catal.* **158**, 336 (1996).
32. Gonzalez, M. R., Kobe, J. M., Fogash, K. B., and Dumesic, J. A., *J. Catal.* **160**, 290 (1996).
33. Kobe, J. M., Gozatez, M. R., Fogash, K. B., and Dumesic, J. A., *J. Catal.* **164**, 459 (1996).
34. Lunsford, J. H., Sang, H., Campbell, S. M., Liang, C.-H., and Anthony, R. G. *Catal. Lett.* **27**, 305 (1994).
35. Mastikhin, V. M., Nosov, A. V., Filimonova, S. V., Terskikh, V. V., Kotsarenko, N. S., Schmachkova, V. P., and Kim, V. I., *J. Mol. Catal. A: Chem.* **101**, 81 (1995).
36. Batamack, P., Doremieux-Morin, C., Fraissard, J., and Freude, D., *J. Phys. Chem.* **95**, 3790 (1991).
37. Batamack, P., Doremieux-Morin, C., and Fraissard, J., *J. Chem. Phys.* **89**, 423 (1992).
38. Batamack, P., Doremieux-Morin, C., Vincent, R., and Fraissard, J., *J. Phys. Chem.* **97**, 9779 (1993).
39. Schnabel, B., Haubenreisser, U., Scheler, G., and Mueller, R., *in* "Proceedings of the 19th Congress Ampere, Heidelberg, 1976" (C. H. Brunner, K. H. Hausser, and D. Schweitzer, Eds.). [Taylor, R. E., Pembleton, R. G., Ryan, L. M., and Gerstein, B. C., *J. Chem. Phys.* **71**, 4541 (1979)]
40. Clearfield, A., Serrette, G. P. D., and Khazi-Syed, A. H., *Catal. Today* **20**, 295 (1994).
41. Somorjai, G. A., *Principles of Surface Chemistry*, pp. 212–222. Prentice-Hall, Englewood Cliffs, NJ, 1972. [*Quantochrome Monorb Instrumentation Manual*, Section I, pp. 1–3, Section III, pp. 1–3, Quantachrome Corp., Boynton Beach, FL.]
42. Fukushima, E., and Roeder, S. B. W., *Experimental Pulse NMR, A Nuts and Bolts Approach*, Addison-Wesley, Reading, MA, 1981.
43. Burum, D. P., Linder, M., and Ernst, R. R., *J. Magn. Reson.* **44**, 173 (1981).
44. Rhim, W. K., Elleman, D. E., and Vaughan, R. W., *J. Chem. Phys.* **59**, 944 (1973).
45. Burum, D. P., and Rhim, W. K., *J. Chem. Phys.* **71**, 944 (1979).
46. Cho, H., *J. Magn. Reson. A* **121**, 8 (1996).
47. Slichter, C. P., *Principles of Magnetic Resonance 3rd ed.*, Springer-Verlag, Berlin, 1990.
48. Smith, S., Levante, T., Meier, B. H., and Ernst, R. R., *J. Magn. Reson. A* **106**, 75 (1994).
49. Yori, J. C., Luy, J. C., and Parera, J. M., *Appl. Catal.* **46**, 103 (1989).
50. Ng, F. T. T., and Horvat, N., *Appl. Catal. A* **123**, 197 (1995).
51. Satterfield, C. N., *Heterogeneous Catalysis in Industrial Practice*, McGraw–Hill, New York, 1991.
52. Chuang, I-S., Kinney, D. R., and Maciel, G. E., *J. Amer. Chem. Soc.* **115**, 8695 (1993).
53. Liu, C. C., and Maciel, G. E., *J. Amer. Chem. Soc.* **118**, 5103 (1996).
54. Kinney, D. R., Chuang, I-S., and Maciel, G. E., *J. Amer. Chem. Soc.* **115**, 6786 (1993).
55. Fleischer, U., Kutzelnigg, W., Bleiber, A., and Sauer, J., *J. Am. Chem. Soc.* **115**, 7833 (1993).
56. Huggins, B. A., and Ellis, P. D., *J. Am. Chem. Soc.* **114**, 2098 (1992).
57. Smith, D. K., and Newkirk, H. W., *Acta Cryst.* **18**, 983 (1965).
58. Pake, G. E., *J. Chem. Phys.* **16**, 327 (1948).